MATERIALE PLASTICE
https://revmaterialeplastice.ro
https://doi.org/10.37358/Mat.Plast.1964

Photodegration of Anionic Dyes Using Polyazomethine/Titanium di-Oxide and Polyazomethine/ Zinc Oxide Nanocomposites

SHANMUGAM JAIGANESH PRADEEBA[1*], BALAKRISHNAN JEYAGOWRI[1], KRISHNASWAMY SIVAKUMAR[2], LAKSHMANA PERUMAL VIDHYA[1], KRISHNAN SAMPATH[3]

[1]Department of Chemistry, Hindusthan College of Engineering and Technology, Valley Campus, Pollachi highway, Othakkalmandapam, Coimbatore-641032, Tamil Nadu, India
[2]Department of Physics, Hindusthan College of Engineering and Technology, Valley Campus, Pollachi highway, Othakkalmandapam, Coimbatore-641032, Tamil Nadu, India
[3]Department of Chemistry, Kumaraguru College of Technology, Coimbatore, Athipalayam Rd, Chinnavedampatti, Coimbatore-641049, Tamil Nadu, India

Abstract: *In this present research work, Poly(azomethine), ZnO, TiO_2, poly(azomethine)/TiO_2 and poly(azomethine)/ZnOnanocomposites were synthesized. Prepared nanocompositewas characterized by FourierTransform-Infrared spectroscopy, UV-Visiblespectroscopy, PowderX-raydiffraction, band gap, EDAX and SEM. The Photocatalytic activity of the samples was evaluated for the degradation of MethylorangeandAlizarin red S under natural sunlight. The effects of dye concentration were studies for the decolorization of MethylorangeandAlizarin red S. The degradationefficiency,reactionkinetics and isotherm studies revealed that the Polyazomethine /ZnO(PNZ) and poly(azomethine)/TiO_2(PNT) nano-composites have shown excellent photocatalytic activity than PAZ, ZnO and TiO_2.At optimum dye concentrations of 10ppm Methyl orange and Alizarin Red S shows maximum degradation efficiency was 87% and 86% usingPNZ and PNT nanocomposites asaphotocatalysts at 5 h contact time. FT-IR, UV-Visible spectroscopy, SEM and EDAX were used to describe the samples after the photocatalytic investigation. To examine the effect of decolorisation of dyes using synthesized photocatalysts Pseudo first order kinetic, pseudosecond order model, Langmuir, Freundlichisothermsstudieswere carriedout and also followed by intra-particle diffusion model, whereas diffusion is not only the rate-controlling step. The results show that the degradation capacity decreases with an increase in solution temperature from303 K to 333 K. The thermodynamics parameters were evaluated.*

Keywords: *polyazomethine, photocatalyst, nanocomposites, anionic dyes, kinetic model, degradation efficiency*

1.Introduction

Environmental pollution coming from organic pollutants and toxic waste water has drawn increasing attention in recent years. Chemical pollution from heavy metals, solvents, dyes, pesticides, and other sources is a severe danger to water quality. These are the major organic pollutants which can cause severe environmental disruption and health damage [1]. Dye waste water from textile industries makes important contribution to serious environmental pollution. Synthetic dyes have a huge ecological impact, as they can alter the physical and chemical properties of water, causing harm to aquatic vegetation and fauna. Dyes containing waste water, for example, decrease light penetration and may hinder photo-synthesis. Wastewater containing dyes from textile industry is very difficult to treat using conventional wastewater treatment methods. Therefore, the dyes decolourisation has been interested by heterogeneous photocatalysis process. Conventional methods such as physical methods, chemical methods or their combinations are used for decolourisation of these dyes. The most adaptable and successful method for eliminating harmful heavy metal ions and organic contaminants from waste water is adsorption and photocatalytic degradation [2].

Recently Advanced oxidation processes (AOPs) was the major cost-effective treatment approach for eliminating dyes from industrial waste water. Bright coloured dyes such as green, blue and brown was

**email: pradeebasj@gmail.com*

most used globally. However, the chemicals employed in dye manufacturing are frequently poisonous, carcinogenic or unstable. As a result, they are unsuitable from an ecological perspective [1-5].

Eventhough advanced oxidation has been shown to be a successful method of treating industrial wastewater discharge. Heterogeneous photocatalysis process revealed that it was most promising essential methods for metallizing organic pollutants completely.

Poly(azomethine)s or Schiff bases or conjugated polymers, suggest a broad range of usage in electronics, optoelectronics and photonics and are particularly appealing because of their structure-function relationship [30]. Several challenges have been made to remove dyestuffs in the past with PANI/TiO_2nanocomposites performing superior photocatalytic activity and strength than bare TiO_2 in the liquid phase deprivation of methylorange and malachitegreen under both UV and Visible irradiation. Polyaniline doped with $SrTiO_3$ nanocubes were prepared using this technique to eliminate Methylene-blue beneath visible radiation [1-8].

Photocatalytic mechanism

The following is a summary of the photocatalytic oxidation pathway (Figure 1) utilising semi-conducting materials:

(i) Photoexcitation: When a photoelectron is promoted from the filled valence band of a semiconductor photocatalyst, such as TiO_2, to the empty conduction band as a result of irradiation, a photocatalytic reaction is activated. The energy (hv) of the absorbed photon is equal to or greater than the band gap of the semiconductor photocatalyst [38]. The valence band (h_{VB}^+) is left with a hole due to the excitation process. As a result, an electron and hole pair (e/h^+) is created, as shown in the equation below.

(ii)Ionization of water: The$OH^{\cdot}$ radical is formed when photogenerated holes in the valence band react with water.

The $OH^{\cdot}$ radical that forms on the irradiation semiconductor surface is a powerful oxidizer. It non-selectively targets adsorbed organic molecules or those that are very close to the catalyst surface, causing them to mineralize to a level determined by their structure and level of stability. It can easily attack not just organic pollutants, but also microorganisms for better decontamination.

(iii) Oxygenionosorption: While the photogenerated hole (h_{VB}^+) reacts with surface bound water or OH^- to produce the hydroxyl radical, electron in the conduction (e_{CB}^-) is taken up by the oxygen in order to generate anionic superoxide radical (O_2^-).

This superoxide ion may not only take part in the further oxidation process but also avoids the electron-hole recombination, thus maintaining electron neutrality within the TiO_2 molecule [39].

(iv) Protonation of superoxide: The superoxide ($O_2^{-\cdot}$) produced gets protonated forming hydro-peroxyl radical ($HO_2^{\cdot}$) and then consequently H_2O_2 which further separates into highly reactive hydroxyl radicals ($OH^{\cdot}$).

On the surface of a photoexcited semiconductor photocatalyst, oxidation and reduction processes are regularly observed.

Therefore a semiconductor photocatalyst can take part in a redox reaction upon photo-excitation on its surface effectively. The general scheme of a photocatalytic reaction involving a semiconductor material used for the dye degradation is as follows (eq. 2 to 8):

$$Dye + h\nu \longrightarrow Dye^{*} \quad (2)$$

$$Dye^{*} + TiO_2 \longrightarrow Dye^{\cdot+} + TiO_2 \quad (3)$$

$$TiO_{2(e)} + O_2 \longrightarrow TiO_2 + O_2^{\cdot-} \quad (4)$$

$$O_2^{\cdot-} + TiO_{2(e)} - 2H^{+} \longrightarrow H_2O_2 \quad (5)$$

$$H_2O_2 + TiO_{2(e)} \longrightarrow OH^{\cdot} + OH^{-} \quad (6)$$

$$Dye^{\cdot+} + O_2\,(O_2^{\cdot-} \text{ or } OH^{-}) \longrightarrow \text{Organic intermediates} \quad (7)$$

$$\text{Organic intermediates} \rightarrow \text{Degraded or mineralized products} \quad (8)$$

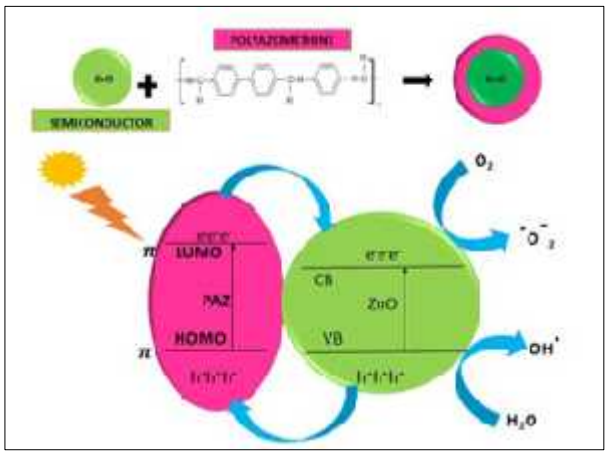

Figure. 1. Photocatalyst mechanism

The present work was carried out using poly (azomethine)PAZ, TiO_2, ZnO, PNT and PNZ nano-composites and structural characterization techniques such as FT-IR,UV-Vis, SEM, XRD and EDAX was done. In the presence of natural sunlight, photocatalytic tests with poly(azomethine)PAZ/ TiO_2(PNT) and PAZ/ZnO(PNZ) nanocomposites were carried out for the removal of methylorange (MO) and Alizarinred S(ARS) existing in wastewater. Photocatalyst deprivation efficiency was measured and agraphwas plotted.

2. Materials and methods

All the chemicals and reagents used in this study were of analytical grade with high purity. The chemicals used in the present study are 4,4'-diformylbiphenylmonomer, dimethyl formamide, *p*-phenylenediamine, methanol, potassium hydroxide, Zinc Nitrate, titanium tetrachloride, ammonium hydroxide and toluene. The Schematic diagram of the methodology of present research work was depicted in the Figure 2.

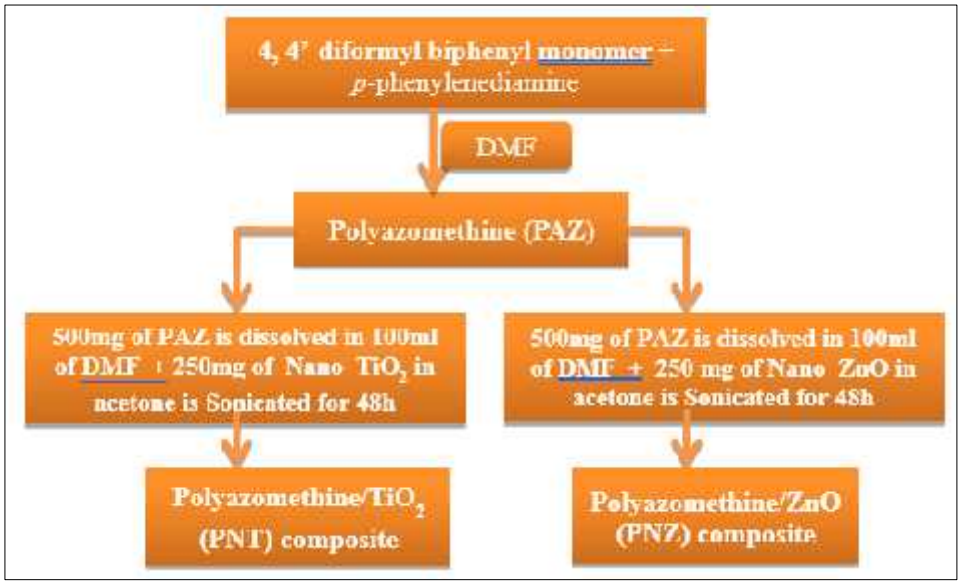

Figure 2. Schematic diagram of the methodology

2.1. Synthesis of polyazomethine (PAZ)

The polymer synthesis is based on the reference work carried out by B Joy vasanthi in 2013 [24]. About 0.5 mol of 4, 4'-diformyl biphenyl monomer is taken in DMF medium added slowly into a mixture of toluene solution of 0.5 mol*p*-phenylenediamine. The contents of the reaction were refluxed for 6 h and then allowed to cool before being discharged into methanol. The resultant precipitate was filtered and dried (Figure 3).

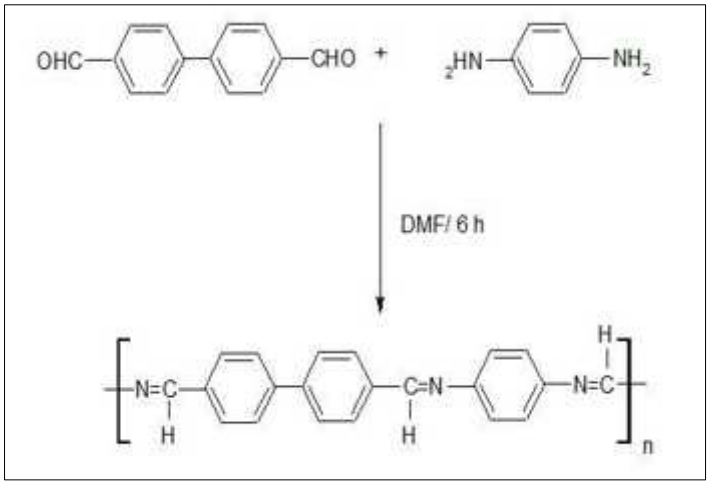

Figure 3. Synthesisof polyazomethine(PAZ)

2.2. Synthesis of ZnO nanoparticle

Under vigorous stirring, an aqueous solution of KOH (0.4 M) is gradually discharged into a zinc nitrate solution (0.2 M) at room temperature, resulting in the formation of a white suspension. After being rinsed three times with filtered water, the whitish substance was centrifuged. The finished product was then cleaned in pure alcohol before being calcined at 500^{o}C for 3 h.

2.3. Synthesis of TiO_2 nanoparticle

In an ice bath, $TiCl_4$ was gradually added to clean water with stirring until it was entirely dissolved simultaneously add NH_4OH (30%) solution was added. After 1 h, the white TiO_2 nanoparticle was filtered. Obtained TiO_2 nanoparticles were washed in clean water and dehydrated for 3 h under vacuum at 100°C.

2.4. Synthesis of ZnO/TiO_2 incorporated polyazomethine polymeric nanocomposite

500 mg polyazomethine is dissolved in 100 mL DMF solution and sonicated for 48 h under constant stirring. Under sonication bath (Figure 4), ZnO or TiO_2 nanoparticles are liberated in acetone and simultaneously added to the polymeric solution. The precipitated ZnO incorporated polyazomethine (PNZ) or TiO_2 incorporated polyazomethine (PNT) composite material is filtered, washed repeatedly in acetone and dried out (Figure 5) [24]. FT-IR spectroscopy, UV-Vis spectroscopy, scanning electron microscopy, transmission electron microscopy and Energy Dispersive Analysis X-ray powder X-ray diffraction were used to verify the synthesised polyazomethines (PNT & PNZ) [25-31].

Figure 4. Sonication bath

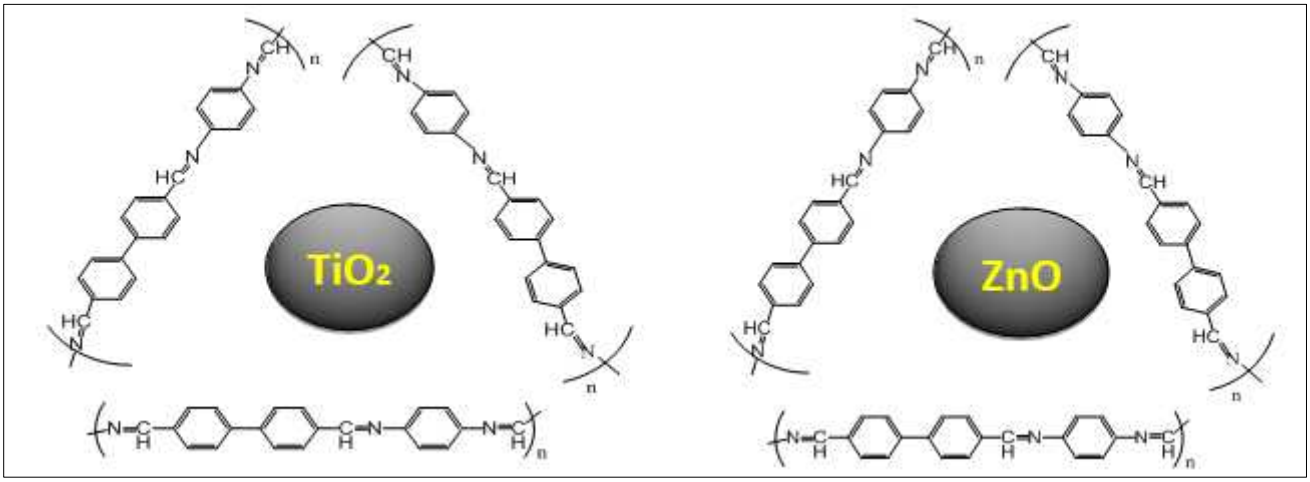

Figure 5. Structure of PNT (left) & PNZ (right) nanocomposite

2.5. Photocatalytic experiment

In the presence of a natural sunlight, batch mode photocatalytic investigations were carried out for the effective degradation of MO and ARS synthetic dyes utilising synthesised photocatalysts (PAZ, PNT, PNZ, TiO_2, and ZnO). Prior to irradiation, the suspension (50 mL dye solution + 20 mg photocatalyst) is stirred for 30 min with a magnetic stirrer (300 rpm) until adsorption-desorption equilibrium is reached. To attain effective photodegradation, the suspension was kept in natural sunlight irradiation after reaching adsorption-desorption equilibrium. A UV-Visible spectrophotometer was used to measure the absorbance of the dye solution, which was pipetted out once at periodic intervals. The photo deprivation efficacy R (%) was calculated using the equation (4):

$$R(\%) = \frac{C_0 - C_t}{C_0} \quad (9)$$

C_0 symbolizes the dye concentration before irradiation and C_t indicates the dye concentration after a set period of time.

2.5.1. Effect of initial dye concentration

50 mL of MO and ARS dyes with concentrations of 10 ppm, 20 ppm, 30 ppm, 40 ppm, and 50 ppm were utilised to analysis the effect of initial dye concentration in optimized *p*H conditions for the time period of 1-5 h with 100 mg of synthesized photocatalysts (PAZ, TiO_2, ZnO, PNT and PNZ).

3. Results and discussions

3.1. Characterization of photocatalyst

3.1.1. Fourier transform-infra red spectroscopy

The FT-IR spectrum of synthetic photocatalysts is discussed in the table below (Table 1). There is no significant change in FT-IR spectra after photodegradation. Minor changes in the peaks are caused by the absorption of methyl orange and alizarin red S. (Figure 6).

Table 1. List of FTIR bands and related group presence in photocatalysts

S.No.	Wavenumber cm^{-1}	Group presence
1	1512cm^{-1}	azomethine linkage (-CH-N)
2	3736 cm^{-1}	N-H stretching vibration
3	3555 cm^{-1}	C-H stretching in aromatic ring
4	1387 cm^{-1}& 1352 cm^{-1}	C=C stretching in benzene ring
5	500 cm^{-1} to 600 cm^{-1}	stretching vibration frequency of $TiO_2$and ZnO
6	1629 cm^{-1}	H–O–H bending vibration
7	2863 cm^{-1}	C–H bond
8	2924 cm^{-1}& 2843 cm^{-1}	C–H stretching vibration of the alkane groups

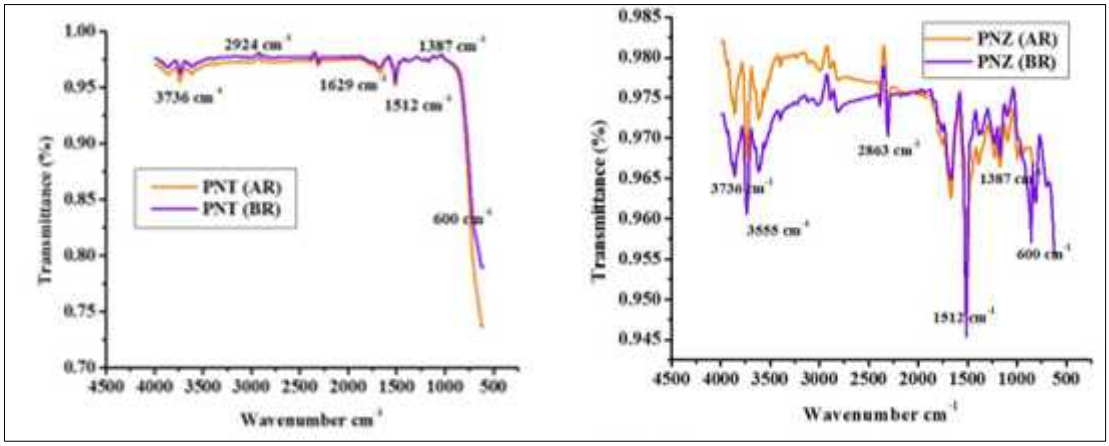

Figure 6. Fourier Transform Infrared spectrumof PNT & PNZ nanocomposite before (BR) and after (AR)elimination of anionic dyes

3.1.2. UV-Visible spectroscopy

In the tabular column below, the UV-Vis spectrum of synthesised photocatalysts is shown (Table 2).

Table 2. List of UV-Vis bands & related group presence in photocatalysts

S.No.	Wavelengthnm	Group presence
1	400 nm to 460 nm	π-π* and n- π* transition between the benzenoid segments

2	490 nm to 500 nm	Electron move from valence band to the antibonding π-π* type of PAZ
3	510 nm to 700 nm	
4	215 nm and 280 nm	TiO_2 nanoparticle
5	375 nm	ZnO nanoparticle

The peak intensity was higher (Figure 7), indicating the presence of auxochrome groups such as –NH_2 and –O in the structure. As a result, visible light or existing natural sunlight illumination can be used to photo-stimulate the produced nanocomposite, which has no harmful effects on human health [31-34].

After the photocatalytic process, the UV-Vis spectra of photocatalysts were studied. The absorption band in the visible region between 400 nm and 700 nm is caused by the removal of methyl orange and alizarin red S dye present in water [11,12].

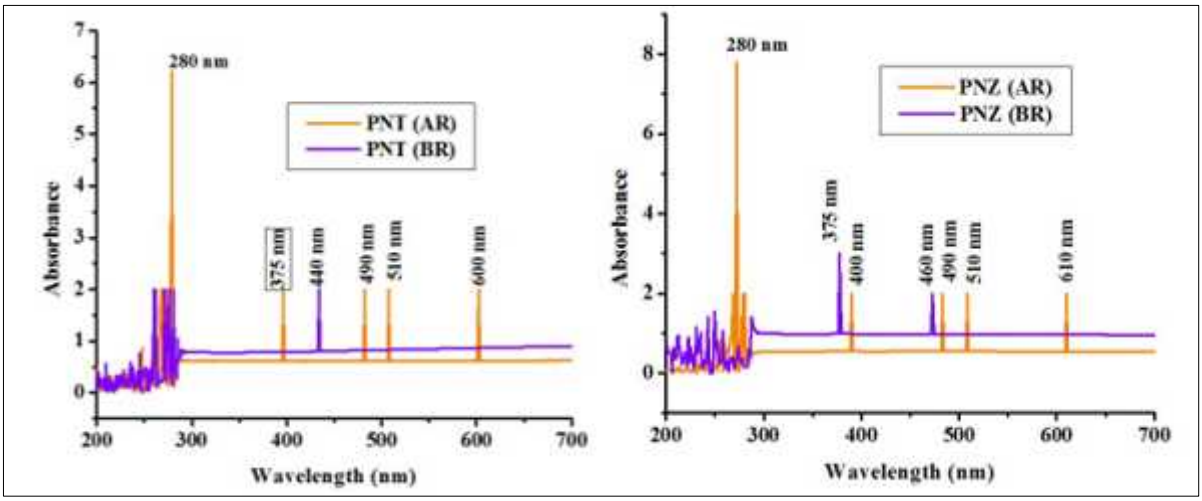

Figure 7. Ultraviolet Visible spectrumof PNT & PNZ nanocomposite before (BR) and after (AR)elimination of dyes

3.1.3. X-Ray diffraction

The XRD characterization studies of synthesized photocatalysts materials were explained in the below tabular column (Table 3).

Table 3. List of XRD peaks & element present in photocatalysts

S.No.	2θ Values	Intrepretation
1	Sharp narrow peaks in PAZ	Recommend the material is crystalline with a little amorphous component.
2	26.27, 31.80, 36.31, 42.04, 47.24, 52.28, 57.82, 62.23, 67.89, 73.23	anatase phase TiO_2
3	29.21, 35.27, 40.08, 44.27, 49.09, 58.19, 63.67,70.40	ZnO with hexagonal crystal structure

The XRD pattern of ZnO the peaks are present in polyazomethine matrix and confirms the formation of PNZ nanocomposite (Figure 8).

The XRD model of TiO_2 depicts diffraction peaks at 2θ values of 26.27, 31.80, 36.31, 42.04, 47.24, 52.28, 57.82, 62.23, 67.89, 73.23 which might be assigned to the anatase phase in the TiO_2 (JCPDS-87-

0598) [5]. The same peaks are present in polyazomethine matrix and confirm the formation of PNZ nanocomposite (Figure 8). The particle size of photocatalysts synthesized was listed in the table below (Table 4).

Table 4. List of Photocatalysts & their particle size

S.No.	Photocatalysts	Particle Size
1	PAZ	65nm
2	TiO_2	29nm
3	ZnO	32nm
4	PNT	30nm
5	PNZ	33.5nm

After study there is no change in XRD pattern (Figure 8) of PNT & PNZ nanocomposite shows the stability of the synthesized photocatalyst.

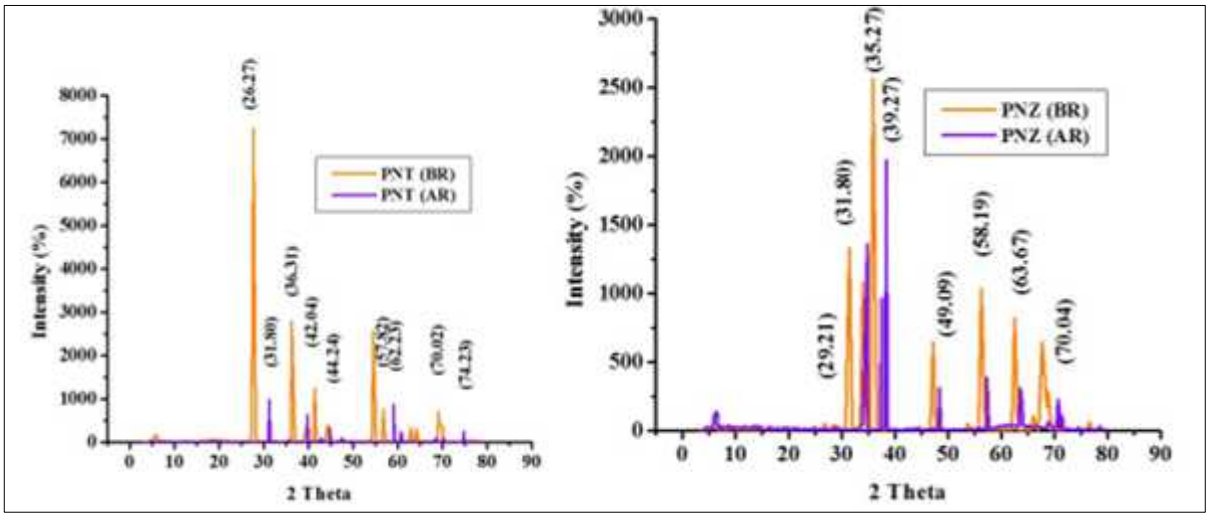

Figure 8. X-ray diffraction peaks of PNT & PNZ nanocomposite before (BR) and after (AR) elimination of dyes

3.1.4. Morphological studies

The SEM and EDAX image of PNT and PNZ nanoparticles before and after photocatalyticstudy have been examined which was represented in the Figure 9-11.

The SEM image (Figure 11) confirms the adsorption of dye molecules on the surface of the photocatalysts. After degradation, changes in the elemental composition and the presence of new elements were found in the EDAX spectrum (Figure 9, 10) which confirms the dyestuffs adsorbed on the catalysts surface [35].

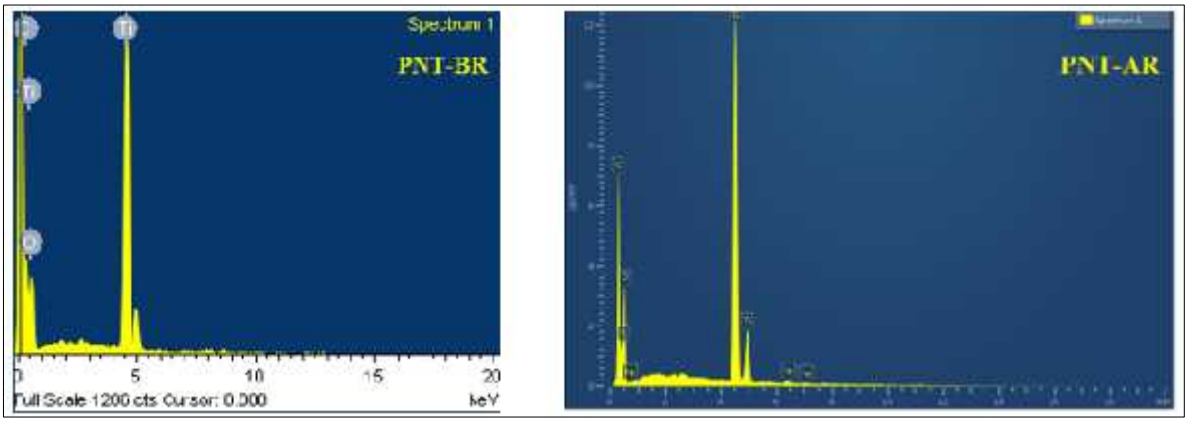

Figure 9. EDAX model of PNT nanocomposite before (left) and after (right) elimination of dyes

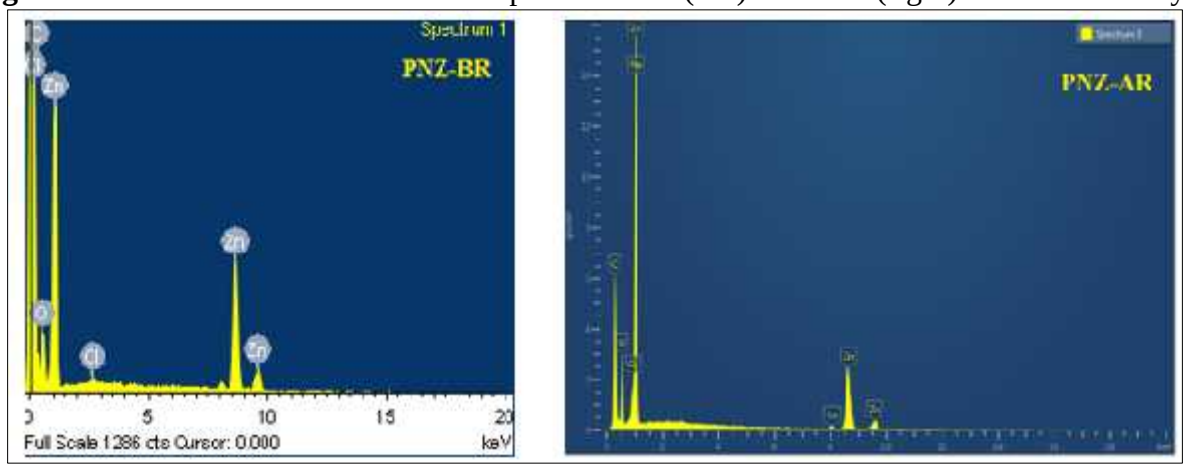

Figure 10. EDAX model of PNZ nanocomposite before (left) and after (right) elimination of dyes

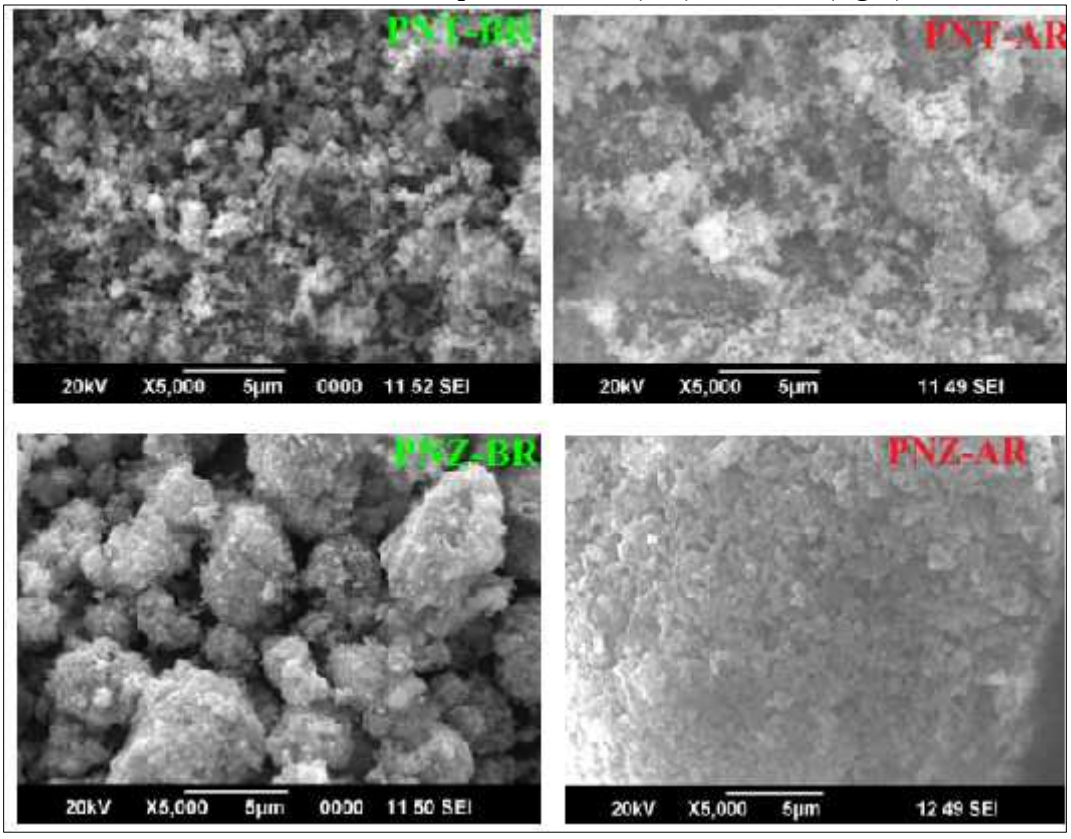

Figure 11. Scanning Electron Microscope image of PNT & PNZ nanocomposite before (BR) and after (AR) elimination of dyes

3.1.5. Band gap of synthesized photocatalysts

From the Tauc plot of αhν (eV^2 m^{-2}) against Photon energy (eV) (Figure 12-14) the band gap energy of PAZ, TiO_2, ZnO, PNT and PNZ were calculated (Table 5).

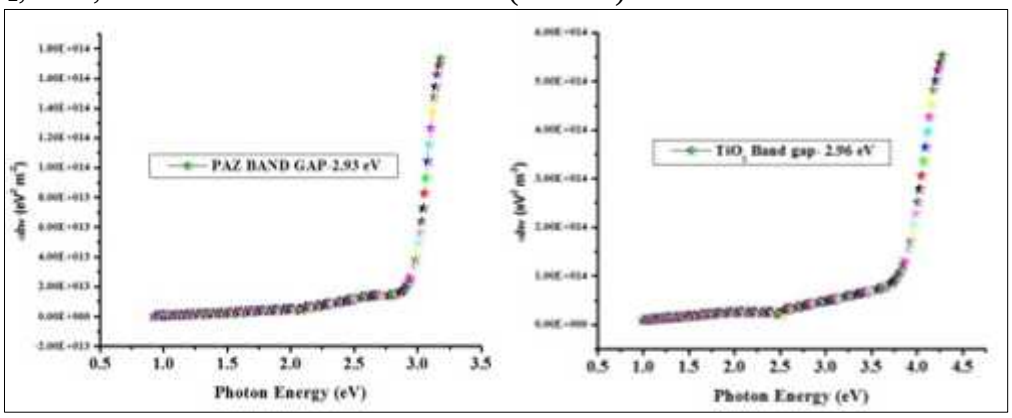

Figure 12. Band gap plot of PAZ (left) & TiO_2 (right)

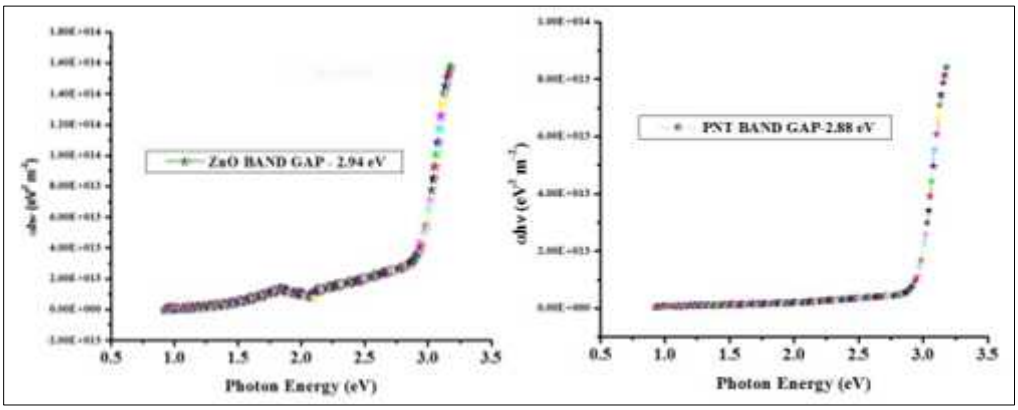

Figure 13. Band gap plot of ZnO (left) & PNT (right)

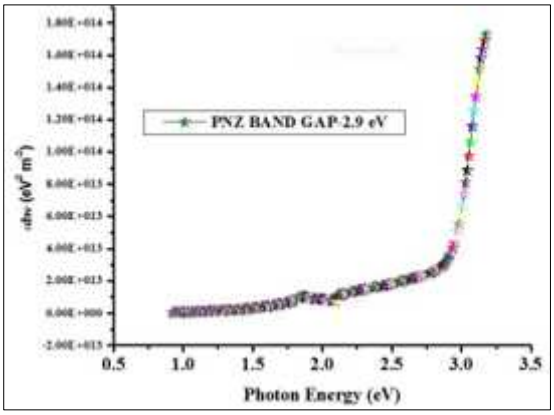

Figure 14. Band gap plot of ZnO (left) & PNT (right)

Table 5. Calculated Bandgap energy of the synthesized materials used for dye degradation

S.No.	Synthesized materials	Wavelength (nm)	Band gap (eV)
1.	PAZ (Azomethine polymer)	530	2.93
2.	TiO_2 Nanoparticles	380	2.96
3.	ZnO Nanoparticles	483	2.94

4.	PNT (Polymeric nanocomposite)	665	2.88
5.	PNZ (Polymeric nanocomposite)	760	2.9

It was observed that the calculated band gap energy of PNT and PNZ was found to be 2.89 eV and 2.9 eV respectively which was lower than the corresponding TiO_2 and ZnO nanoparticles calculated band gap 2.96eV and 2.94 eV. Therefore, addition of PAZ polymer onto TiO_2 and ZnO matrix resulted in the red shift in the wavelength of the adsorption to visible region. This shift makes it possible to carry out the photodegradation of dye molecules in the presence of sunlight proving to as visibly active photocatalyst**.** It was discovered that photocatalyst photoabsorption is influenced by electron-hole pair mobility, which determines the frequency of electrons and holes contact reaction sites on the photocatalyst surface.

3.2. Synthesized composite materials photocatalytic activity in the existence of natural sunlight

Batch photocatalytic studies were carried out to determine the effect of variation of initial concentration on the effective removal of MO and ARS at a given dosage of photocatalysts at 100 mg at time interval between 1 to 5 h [9-11].An increased amount of photocatalyst ranging from 10 ppm to 50 ppm was used to determine the optimum dye concentration for removing MO and ARS.

The exponential variation of the percentage removal of dyes (MO and ARS) with the dose of catalysts (PAZ, PNT, PNZ, TiO_2 and ZnO) is depicted in the Figure 15-24.

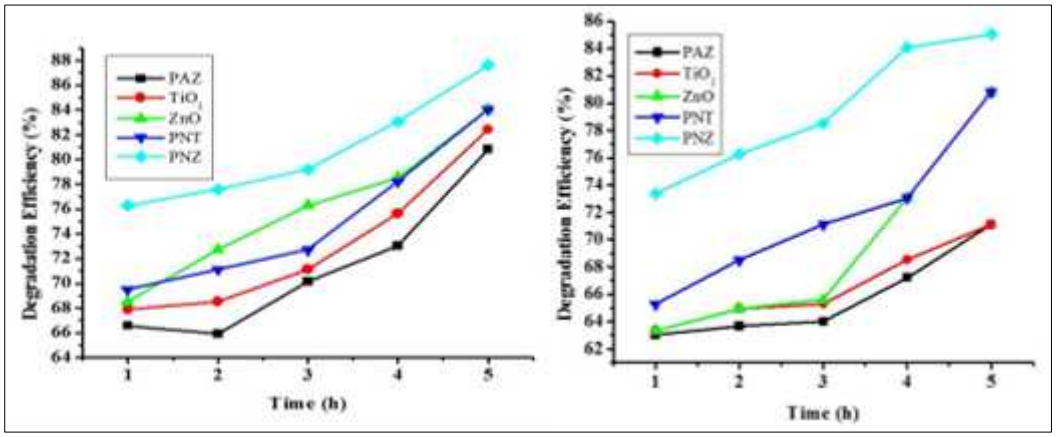

Figure 15, 16. The deprivation efficacy of MO dye in sunlight irradiation with 100 mg catalyst PAZ, ZnO, TiO_2, PNZ& PNT at 10 & 20 ppm dye concentration

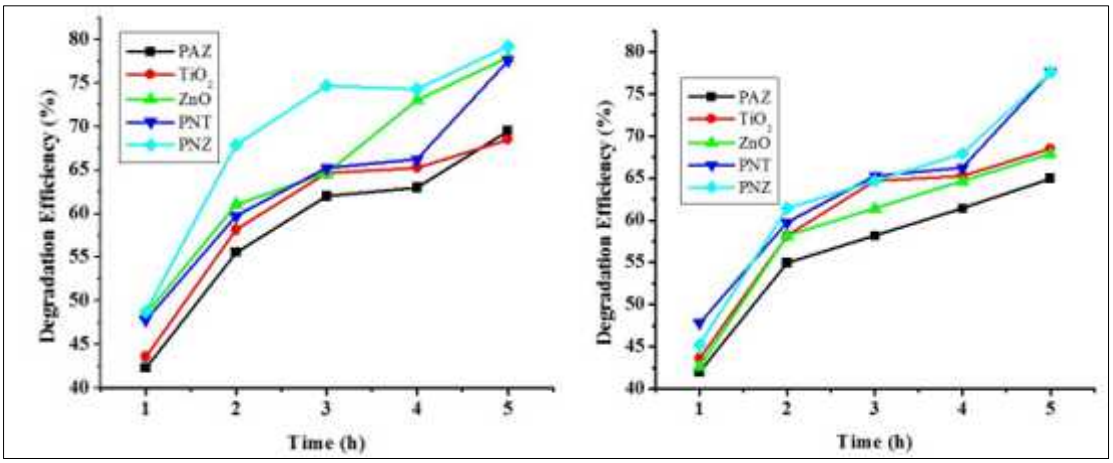

Figure 17, 18. The deprivation efficacy of MO dye in sunlight irradiation with 100 mg catalyst PAZ, ZnO, TiO_2, PNZ & PNT at 30 & 40 ppm dye concentration

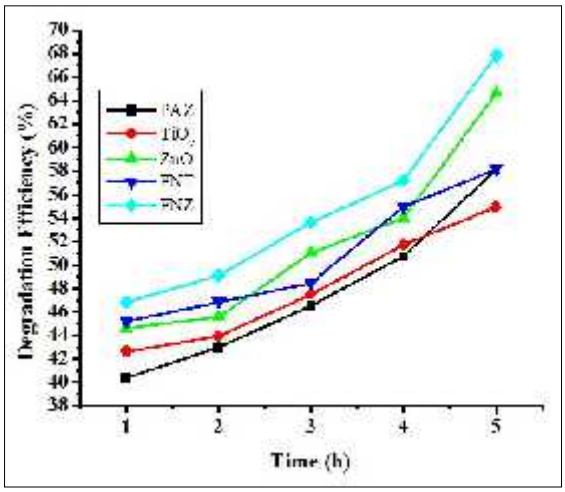

Figure 19. The deprivation efficacy of MO dye in sunlight irradiation with 100 mg catalyst PAZ, ZnO, TiO_2, PAZ/ZnO (PNZ) & PAZ/TiO_2 (PNT) at 50 ppm dye concentration

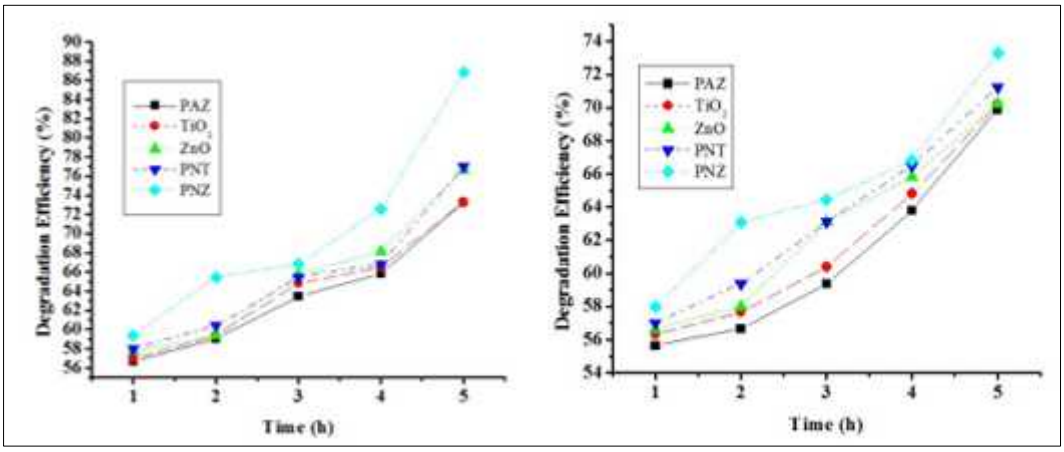

Figure 20, 21. The deprivation efficacy of ARS dye in sunlight irradiation with 100 mg catalyst PAZ, ZnO, TiO_2, PNZ & PNT at 10ppm & 20 ppm dye concentration

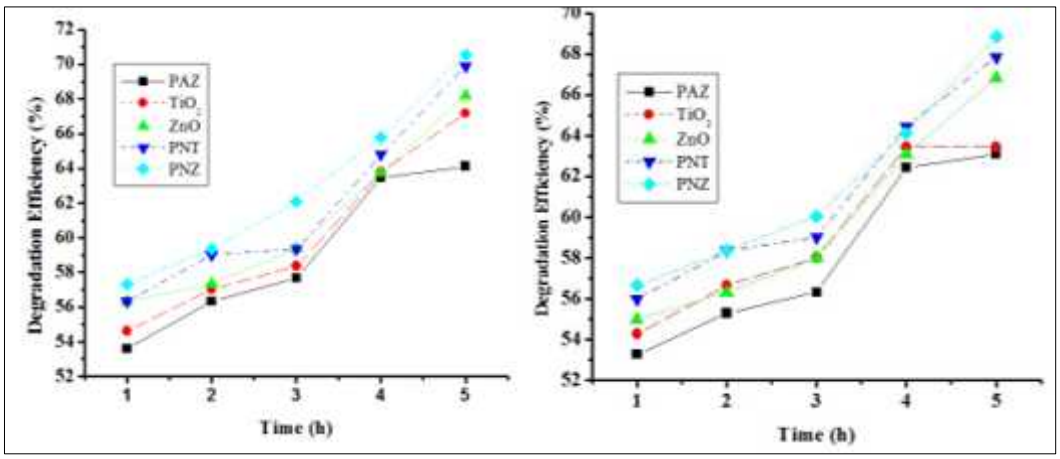

Figure 22, 23. The deprivation efficacy of ARS dye in sunlight irradiation with 100 mg catalyst PAZ, ZnO, TiO_2, PNZ & PNT at 30 & 40 ppm dye concentration

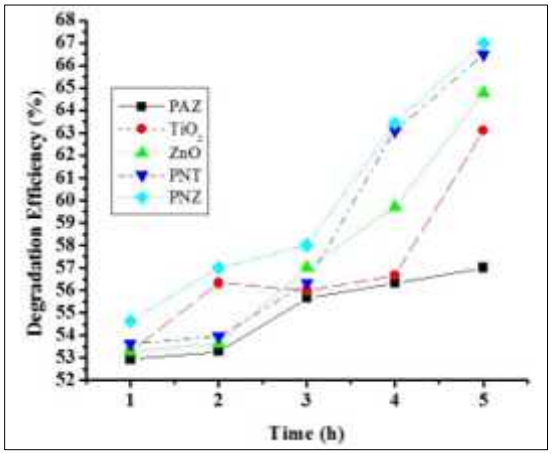

Figure 24. The deprivation efficacy of ARS dye in sunlight irradiation with 100 mg catalyst PAZ, ZnO, TiO_2, PNZ & PNTat 50 ppm dye concentration

The results reveal that when the initial dye concentration increases, the degrading effectiveness of MO and ARS decreases. As the initial concentration of a dye solution rises, less light may reach the catalyst's surface, resulting in a decrease in the dye molecules activation [36,37].

The maximum degradation efficiency of MO and ARS at 5 h was depicted in the Table 6 and it was represented in the Figure 15-24. The order of degradation efficiency of photocatalysts in removal of dyes was as follows,

$$PNZ > PNT > ZnO > TiO_2 > PAZ$$

Table 6. Maximum degradation of photocatalysts

Dosage-100mg, 10 ppm, contact time - 5 h					
METHYL ORANGE DEGRADATION DEFFICIENCY (%)					
	PAZ	TiO_2	ZnO	PNT	PNZ
10ppm	80.82	80.44	81.06	81.06	87.00
20ppm	71.11	71.11	80.82	80.82	85.03
30ppm	69.49	68.52	77.91	77.58	79.20
40ppm	64.96	68.52	67.87	77.58	77.58
50ppm	58.17	54.93	64.64	58.17	67.07
ALIZARIN RED S DEGRADATION DEFFICIENCY (%)					
	PAZ	TiO_2	ZnO	PNT	PNZ
10ppm	73.27	73.27	76.66	77.00	86.31
20ppm	69.88	70.22	70.22	71.24	73.27
30ppm	64.12	67.17	68.19	69.88	70.56
40ppm	63.10	63.44	66.83	67.85	68.86
50ppm	57.00	63.10	64.80	66.49	67.00

The maximum degradation efficiency percentage reached to 87% in the removal of MO and 86% in the removal of ARS. From these studies, optimum dye was found to be 10ppm. In comparison to ZnO, TiO_2, PAZ, the PNZ and PNT nanocomposite shows an efficient photocatalyst material.

The degradation efficiency was compared with few photocatalyst materials listed in the Table 6. Since the intensity of UV light in stimulated remains constant throughout the experiment because it is highly focused, so the maximum degradation efficiency >90% was obtained using stimulated UV-

Visible radiation and stimulated solar radiation, whereas the intensity of natural sunlight may vary due to weather conditions.

3.3. Kinetic studies

The kinetics, rate of degradation efficiency of MO, ARS and the mechanism of photocatalytic process of these morphologies of PAZ, PNT, PNZ, TiO_2 and ZnO was studied. It also gives the factors that affect the speeds of a chemical reaction. Chemical kinetics study elucidates detailed observations of the experimental conditions that influence the rate of a chemical reaction and aid in the attainment of equilibrium in a reasonable time [38].

The kinetics of the photo degradation process was explored using two kinetic models, pseudo first order and pseudo second order, because photocatalytic process is considered as important in heterogeneous conditions. These models elucidated in the following section.

3.3.1 Pseudo first order kinetic model

The pseudo first order kinetiuc equation,

$$\ln C_0 / C_t = K.\ t + C \qquad (10)$$

C_0 is initial concentration of MO and ARS, C_t is the concentration of dyes at a differnt contact time t, K is the pseudo first order rate constant (min^{-1}).

The pseudo second order kinetic model is,

$$t/\ q_t = 1/K_2 q_e + t/q_e \qquad (11)$$

q_t is the amount of dye removal at time t, q_e is the amount of dye removal at equilibrium, K is the pseudo second order rate constant (min^{-1}).

A straight line plot of $\ln C_0/C_t$ versus time for pseudo first order reaction and t/q_t versus time for pseudo second order reaction using photocatalysts (PAZ, PNT, PNZ, TiO, and ZnO) was shown in Figure 25-26.

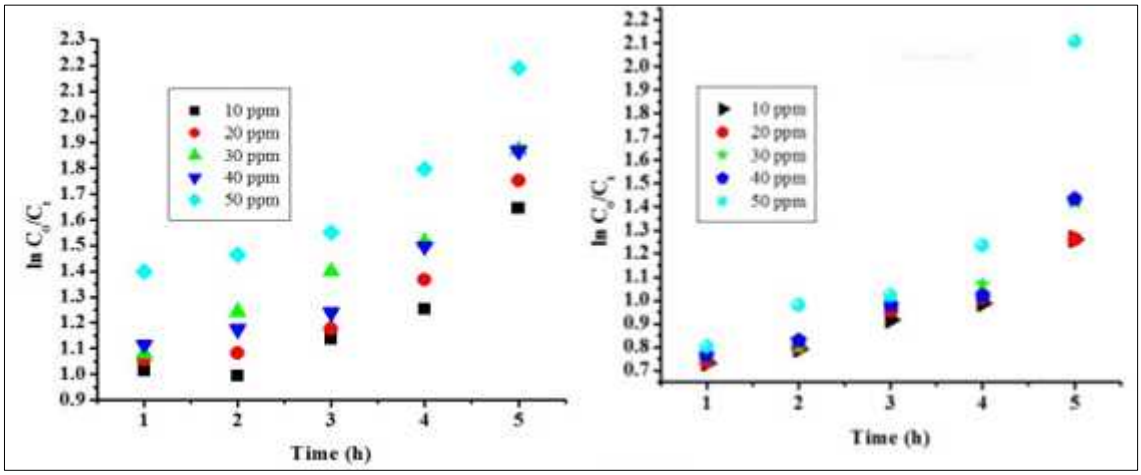

Figure 25. Pseudo first order kinetics for the removal of MO (left) and ARS (right) by photocatalysts

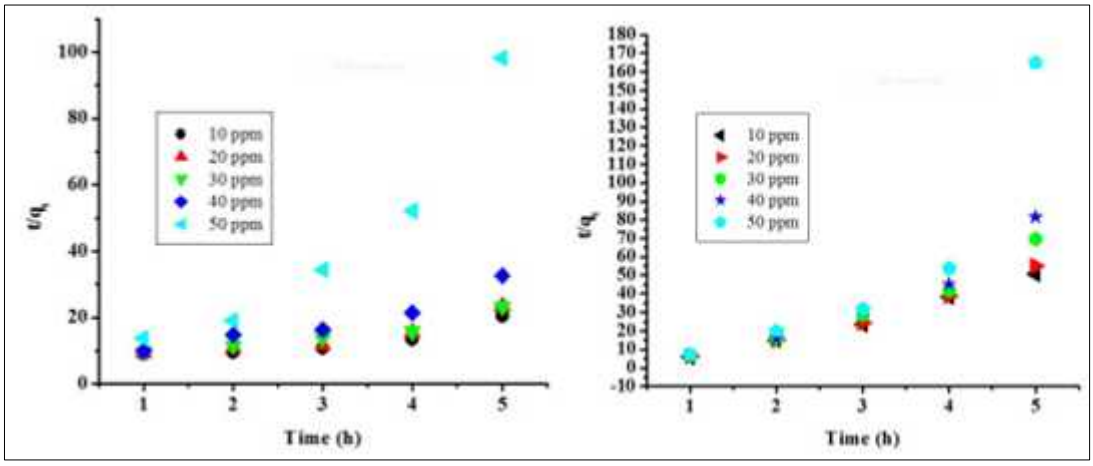

Figure 26. Pseudo Second order kinetics for the removal of MO (left) and ARS (right) by photocatalysts

Table 7. Kinetic model results for degradation of anionic dyes using Photocatalysts

	Methyl Orange						Alizarin Red S					
	Pseudo first order			Pseudo Second order			Pseudo first order			Pseudo Second order		
Dye variation	Intercept	Slope	r-value	Intercept	Slope	r-value	Intercept	Slope	r-value	Intercept	Slope	r-value
10ppm	1.121	0.121	0.993	6.217	2.31	0.904	0.709	0.016	0.995	5.626	0.313	0.92
20ppm	0.913	0.201	0.998	35.4	18.27	0.895	0.907	0.024	0.969	50.67	3.368	0.899
30ppm	0.402	0.033	0.911	12.54	1.792	0.914	0.698	0.02	0.989	47.73	3.079	0.91
40ppm	0.809	0.045	0.991	21.94	20.45	0.963	0.632	0.02	0.995	44.78	0.942	0.942
50ppm	0.549	0.037	0.977	0.193	2.347	0.841	0.631	0.011	0.968	5.551	0.289	0.915

On evaluating the pseudo first order and second order models from Table 7 and Figures 25-26, it is obvious that the pseudo first order model was applicable to the process and that the pseudo second order model was not applicable to the kinetics of the degradation process, as illustrated by the low R values [21]. From the results, pseudo first order fits the process better than pseudo second order.

3.3.2 Langmuir isotherm

For the assessment of the best adsorption ability subsequent to total monolayer coverage on the adsorbent surface, the Langmuir isotherm model was chosen [27].

Langmuir equation is commonly expressed as follows,

$$C_e / q_e = 1/q_m\, C_e + 1/K_a\, q_m \qquad (12)$$

C_e is the dye concentration in solution at equilibrium, q_e is the unit equilibrium adsorption capacity, q_m is the maximum dye uptake, and K_a is a constant denoting the energy of adsorption and affinity of the binding sites providing information on adsorption capacity throughout a monolayer. By plotting $1/q_e$ versus$1/ C_e$values of q_m and K_a can be calculated (Figure 27)

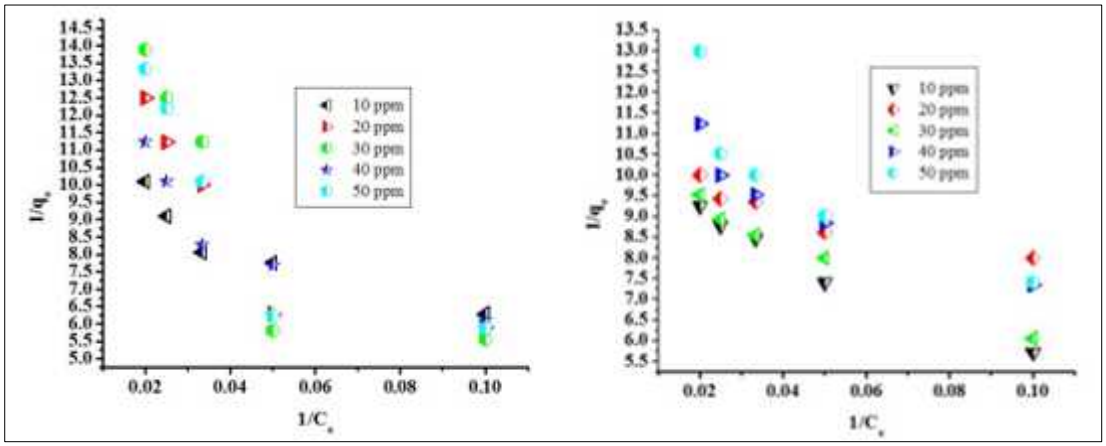

Figure 27. Langmuir isotherm for the removal of MO (left) and ARS (right) by photocatalysts

Table 8. Langmuir isotherm values of Intercept and slope in the removal of Anionic dyes using photocatalysts

Langmuir isotherm						
	Methyl Orange			**Alizarin Red S**		
Dye variation	Intercept	Slope	r-value	Intercept	Slope	r-value
10ppm	6.076	1.145	0.91	7.969	0.402	0.945
20ppm	7.744	1.179	0.987	7.85	0.916	0.892
30ppm	4.762	0.668	0.9106	8.158	0.458	0.971
40ppm	4.742	0.849	0.923	7.117	0.405	0.968
50ppm	4.828	1.037	0.944	5.303	0.406	0.913

A non-dimension constant separation factor or equilibrium parameter R_L, can express the crucial uniqueness of a Langmuir isotherm which is given by,

$$R_L = 1 / (1+ K_L C_e) \quad (13)$$

The influence of isotherm shape on favorable or unfavorable photo-catalytic process has been considered. The R_L ratespecify thatwhether the type of the isotherm were unfavorable (R_L>1), linear (R_L=1), favorable (0<R_L<1) or irreversible (R_L=0). In the present experiment results which were mentioned in the table-8 were found for R_L between 0.892 and 0.987 which clearly indicate the photo-catalytic process was favorable [29].

3.3.2. Freundlich isotherm

The Freundlich equation was demonstrated for the elimination of dyes MO and ARS on the catalyst. The Freundlich isotherm was represented by

$$\text{Log } q_e = \log K_f + 1/n \log Ce \quad (14)$$

where q_e represents the amount of dye removed, C_e represents the solution's equilibrium concentration, and K_f and n represent the elements that change the adsorption capacity and intensity, respectively. The degradation of dyes follows the Freundlich adsorption isotherm, as shown by linear graphs of log qe versus Ce in Table 9 and Figure 28.

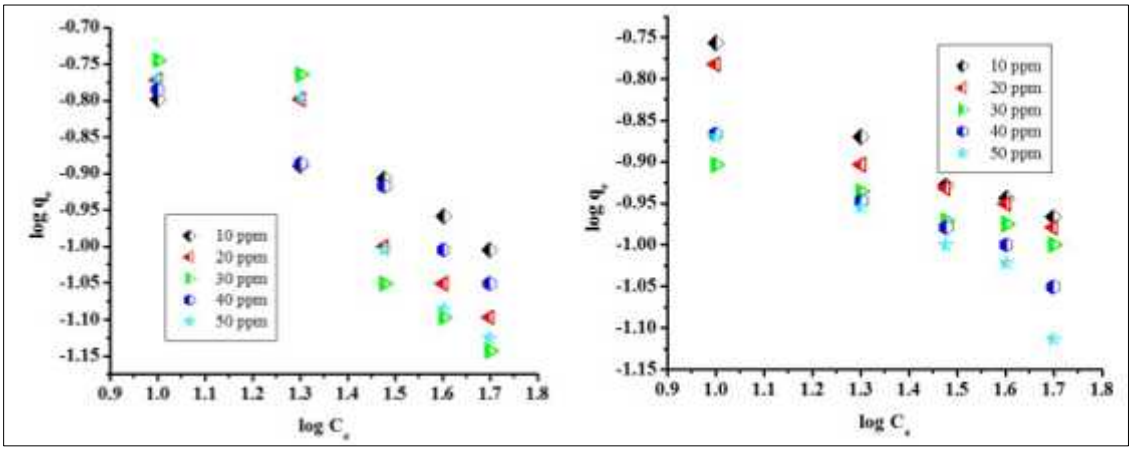

Figure 28. Freundlich isotherm for the removal of MO (left) and ARS (right) by photocatalysts

Table 9. Freundlich isotherm values of Intercept and slope in the removal of Anionic dyes using photocatalysts

Freundlich isotherm						
	Methyl Orange			Alizarin Red S		
Dye variation	K_f	n	R-value	K_f	n	R-value
10ppm	-0.799	-0.008	0.553	-0.915	-0.02	0.976
20ppm	-0.888	-0.029	0.561	-0.904	-0.019	0.942
30ppm	-0.945	-0.031	0.728	-0.742	-0.03	0.61
40ppm	-0.992	-0.03	0.728	-0.857	-0.021	0.92
50ppm	-0.888	-0.029	0.561	-0.912	-0.036	0.915

The values of K_f and n in Table 9 reveal that as negative charges on the photocatalyst surface build, an electrostatic force similar to the vanderwaals force develops between the catalyst surface and the dye.If n is equal to unity, the photocatalytic process is linear; if n is less than unity, the photocatalytic process is chemical; and if n is greater than unity, the photocatalytic process is favourable. From the Table 9, it was found that the degradation process is favorable. The intensity of adsorption is determined by the n value, which reflects the bond energies between dye and photocatalysts as well as the probability of minimal chemisorptions occurs rather than physisorption [37].

3.3.3. Intra-particle diffusion model

The diffusion process could not be identified using the pseudo-first and second order kinetic models, so the kinetic parameters were investigated using the intra-particle diffusion model. The initial rate of intra-particle diffusion is obtained by linearization of equation 15 in the model established by Weber and Morris, McKay and Poots [39],

$$q_t = k_i t^{1/2} + C \quad (15)$$

where C is the intercept and K_i is the intra-particle diffusion rate constant (mg/g $min^{1/2}$).

If intraparticlediffusion is engaged in the adsorption process, the plot of uptake, q_t vs the square root of time ($t^{1/2}$) should be linear, and if these lines pass through the origin, intra-particlediffusion is the rate-controlling step based on this model. When the plots do not pass through the origin, it indicates that there is some degree of boundary layer control, indicating that intra-particle diffusion is not the only rate limiting step, but that other kinetic models may also control the rate of adsorption, all of which may be operating at the same time. The slope of the straight-line parts of the plot of $q_t$versus $t^{1/2}$ for varied solutions temperatures yielded the intra-particle diffusion, K_i values (Figure 29).

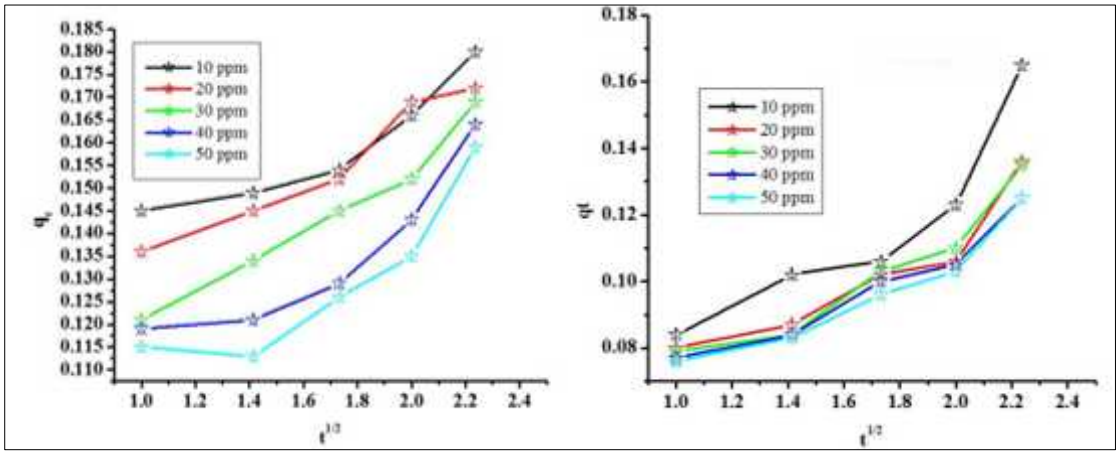

Figure 29. Intraparticle diffusion model of the removal of MO (left) and ARS (right) by photocatalysts

The correlation coefficients (R^2) for the intraparticle diffusion modelare between 0.99 at 25 ºC and decreases by increasing temperature (Table 10).

Table 10. Intraparticle diffusion model for degradation of MO and ARS

C_0(ppm)	Kid	C	R^2
10	0.057	3.3396	0.8838
20	0.0799	3.6957	0.9217
30	0.0989	4.6213	0.9256
40	0.0921	3.5484	0.9613
50	0.0567	3.1229	0.8270

The intra-particlerate constant values (K_i) were found to rise with solution temperature. Porediffusion in sorbent particles was aided by increasing the temperature, which resulted in a faster intra-particle diffusion rate. A considerable number of ions are likely to seep into the pore before being adsorbed. It was discovered that the straight lines did not pass through the origin, implying that intra-particle diffusion is not the only rate-controlling process.

3.3.4. Thermodynamic studies

The thermodynamic studies were performed for the removal of organic dyes using PAZ polymer to check whether the reaction if possible and nature of the reaction rate. The plot of temperature 1/T against log (K_c) was plotted (Figure 30).

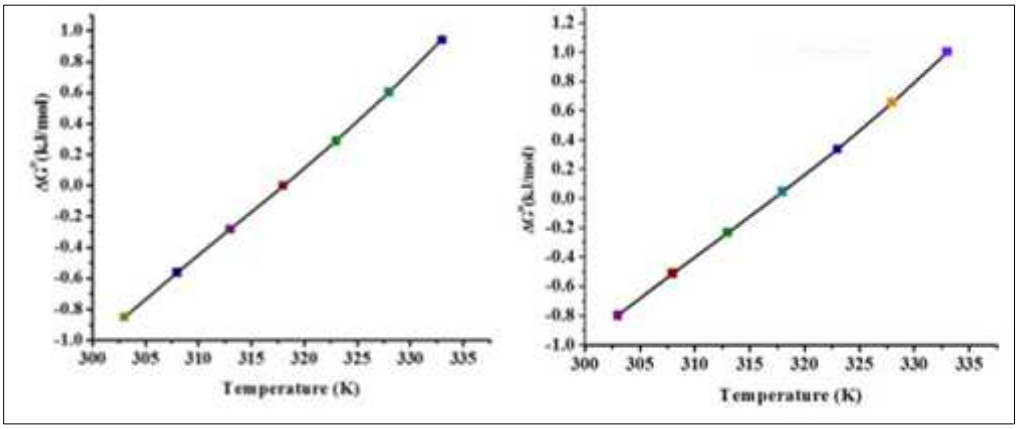

Figure 30. Thermodynamic parameter plot of MO (left) and ARS (right) by photocatalysts

The thermodynamic parameters are calculated and presented in Table 11.

Table 11. Thermodynamic parameter for the decolourization of dyes using PAZ

Dyes (10 mg/L)	ΔH° (kJ/mol)	ΔS° (J/mol/K)	ΔG° (kJ/mol)						
			303 K	308 K	313 K	318 K	323K	328K	333K
MO	-43.19	-135.96	-0.852	-0.562	-0.282	-0.002	0.287	0.602	0.941
ARS	-43.22	-136.41	-0.797	-0.510	-0.232	0.048	0.338	0.657	1.002

From the results, it was evident that with increase in temperature, the decolourization is less favored. The negative values of ΔG, ΔH and ΔS predicts that the decolourization of dyes using PAZ polymer is more favored, spontaneous and the nature of the reaction is exothermic [40].

3.4 Reusability test

The experiments were carried out for a total of 5 cycles at a dye concentration of 50 ppm and a photocatalyst dosage of 100 mg. The photocatalyst is periodically rinsed with double distilled water and dried after each experiment. The recovered photocatalyst is then employed in the following experiment. After 5 cycles, there is no discernible loss of photocatalytic activity, and the modest decline in activity is ascribed to photocatalyst loss during washing (Figure 31) [1]. As a result, the photocatalyst for dye degradation in water is stable and reusable.

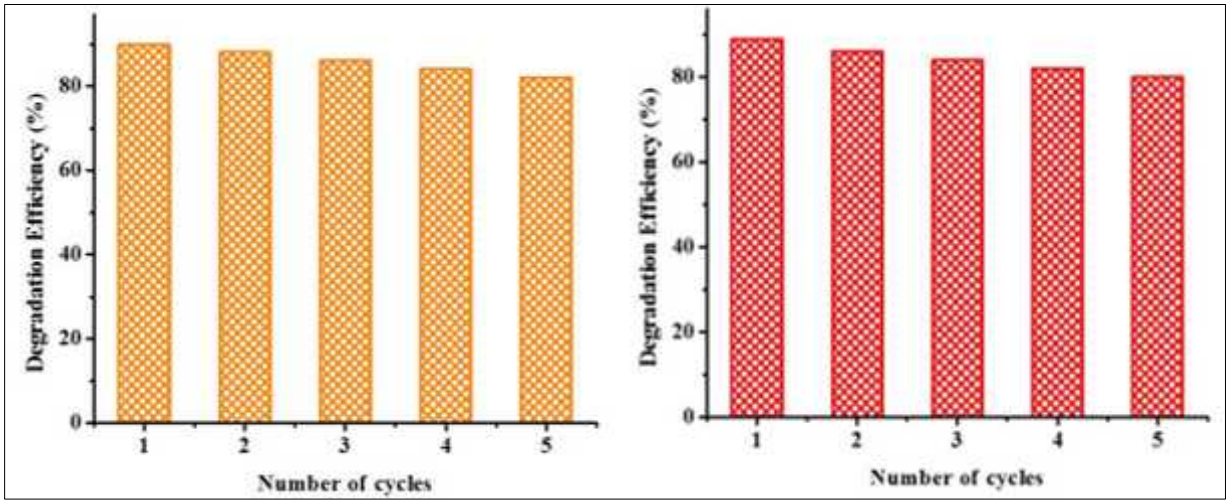

Figure 31. Reusability test for photocatalysts for photodegradation of MO(left) and ARS (right) dye in aqueous phase

4. Conclusions

The photocatalytic removal of dye pollution from textile waste water by PAZ, PNT, PNZ, TiO_2, and ZnO nanocomposites in the presence of natural sunlight was examined in this study. The effects of dye variation were investigated. The effectiveness of MO and ARS degradation reduces as the initial concentration of the dyes increase. In the dye variation investigation, the maximum degradation efficiency were 87 and 86% in the presence of natural sunlight and the optimum dye concentration was 10 ppm at 100 mg photocatalyst dosage.

PAZ, PNT, PNZ, TiO_2, and ZnO nanocomposites were used as a catalyst in the presence of natural sunlight to study kinetic isotherm pseudo first order and pseudo second order for dye variation. The best fit model was found to be pseudo first order based on the graph r-value. Adsorption isotherm Langmuir and Freundlich has been analyzed for dye variation parameter in the removal of anionic dyes (MO and ARS). Graphs have been plotted for each isotherm and intercept, slope, r-value was obtained from them.

From the two isotherm model it was found that Langmuir is the best fit model and from freundlich it was found that slight chemisorptions process was carried out. Also, it was observed that the intra-particle diffusion was not the only rate-controlling step. The negative values of ΔG, ΔH and ΔS predicts that the decolourization of dyes using photocatalyst is more favored, spontaneous and the nature of the reaction is exothermic

Acknowledgement: The authors express their gratitude to the Hindusthan College of Engineering and Technology management and principal for their assistance in completing the project successfully.

References

1.AL-KAHTANI, A. A., Photocatalytic Degradation of Rhodamine B Dye in Wastewater Using Gelatin/CuS/PVA Nanocomposites under Solar Light Irradiation, *Jr. of Biomat. & Nanobiot.*, **8**,2017, 66-82.
2.AMENAGHAWON, N.A., OSARUMWENSE, J.A., AISIEN, F.A., OLANIYAN, O.K., Preparation and Investigation of The Photocatalytic Properties of Periwinkle Shell Ash for Tartrazine Decolourisation, *Jr. of Mech. Engg. & Sci.*, **7**, 2014, 1070-1084.
3.ANSARI, M.O., KHAN, M.M., ANSARI, S.A., CHO, M.H, Polythiophene nanocomposites for photodegradation applications: Past, present and future, *Jr. of Saudi Chem. Soci.*, **19**, 2015, 494–504.
4. ESKIZEYBEK, V., SARI, F., GULCE, H., GULCE, A., AVCI, A., Preparation of the new polyaniline / ZnO nanocomposite and its photocatalytic activity for degradation of methylene blue and malachite green dyes under UV and natural sun lights irradiations, *Applied cat. B: Envi.*, **119**, 2012, 197-206.
5.GOPALAPPA, H., YOGENDRA, K., MAHADEVAN, K.M., MADHUSUDHANA, N., A comparative study on the solar photocatalytic degradation of brilliant red azo dye by CaO and $CaMgO_2$ nanoparticles, *Int. Jr. of Sci. research*, **1**,2012, 91-95.
6 GOVINDHAN, P., PRAGATHISWARAN, C, Synthesis and characterization of TiO_2 @ SiO_2 – Ag nanocomposites towards photocatalytic degradation of rhodamine B and methylene blue, *Jr. of Mat.Sci.*, **1**,2016, 60-65.
7. HUILI, C., CHANG, T., Thermotropic liquid crystalline polymer. III. Synthesis and properties of poly (amide-azomethine-ester) *Jr. of poly. Sci.*, **29**, 1991, 361-367.
8.JENWHANG, T, TAOHSIEH, M., HANCHEN, H, Visible -light photocatalytic degradation of methylene blue with laser –induced Ag/ZnO nanoparticles, *Appl. surface sci.*, **258**, 2012, 2796-2801.
9.JUMAT, N.A, WAI, P.S, CHING, J.J., BASIRUN, W.J, Synthesis of Polyaniline-TiO_2 Nano-composites and Their Application in Photocatalytic Degradation, *Polymers& Poly. Composites*, **25**, 2017, 507-513.
10. KAMIL, A.M., ABDALRAZAK, F.H., HALBUS A.F., HUSSEIN, F.H., Adsorption of Bismarck Brown R Dye onto Multiwall Carbon Nanotubes, *Environ.Analy. Chemis*, **1**, 2014, 1-6.
11.KATANCIC, Z., SUKA, S., VRBAT, K., TASIC, A., HRNJAK-MURGIC, Z., Synthesis of PEDOT/ZnO Photocatalyst: Validation of Photocatalytic Activity by Degradation of Rr45 Dye, *Interna. Symp. on Environ. Management*, **1**, 2016, 67-73.
12.KIM, S.P., CHOI, M., CHOIA, H.M., Photocatalytic activity of SnO_2 nanoparticles in methylene blue degradation, *Mat. Research Bulletin*, **74**,2016, 85–89.
13.LAKSHMIPRASANNA, V., RAJAGOPALAN, V., A New Synergetic Nanocomposite for Dye Degradation in Dark and Light, *Scientific Reports*, **6**:38606,2016, 1-10.
14. LIUXUE, Z., PENG, L., ZHIXING, S., Preparation of PANI- TiO_2 nanocomposites and their solid-phase photocatalytic degradation, *Poly. Degrade. & stab.*, **91**, 2006, 2213-2219.
15.MOOSVI, S.K., MAJIDA, K., ARAA, T., Studying the electrical, thermal, and photocatalytic activity of nanocomposite of polypyrrole with the photoadduct of K_3 $[Fe(CN)_6]$ and diethylenetriamine, *Materials Research*, **2**, 2016, 1-8.

16. MUINDE, V.M., ONYARI, J.M., WAMALWA, B., WABOMBA, J., THUMBI, R.M, Adsorption of Malachite Green from Aqueous Solutions onto Rice Husks: Kinetic and Equilibrium Studies, *Jr. of Environ. Prot.*,**8**, 2017, 215-230.
17. MZOUGHI, M., ANUKU, W., OPPONG, S.O.B, SHUKLA, S.K., AGORKU, E.S., GOVENDER, P.P, Neodymium doped ZrO_2-graphene oxide nanocomposies: A promising photocatalyst for photodegradation of Eosin Y Dye, *Adv. Mat. Let.*, **7**, 2016, 946-950.
18. PATHANIA, D., GUPTA, D., MUHTASEB, A.H., SHARMA, G., KUMAR, A., NAUSHAD, M., AHAMAD, T., ALSEHRI, S.M, Photocatalytic degradation of highly toxic dyes using chitosan-g-poly (acrylamide)/ZnS in presence of solar irradiation, *Jr. of Photochem. & Photobiology A: Chem.*, **329**, 2016, 61-68.
19. PATIL, M.R., SHRIVASTAVA, V.S., Adsorptive removal of methylene blue from aqueous solution by polyaniline-nickel ferrite nanocomposite: a kinetic approach, *Desal. & Water Treat.*, **2**, 2015, 1-9.
20. PATIL, S.P, MAHAJAN, V.K, SHRIVASTAVAA, V.S., SONAWANE, G.H, Kinetics of photocatalytic degradation of Methylene Blue by ZnO-bentonite nanocomposite, *Iran. Chem. Comm.*,**5**, 2017, 417-428.
21. PERJU, E., GHIMPU, L., HITRUC, G., HARABAGIU, V., BRUMA, M., MARIN, L., Organic–inorganic Hybrid Nanomaterials Based on Inorganic Oxides and a Mesomorphicpolyazomethine, *High Perf. Poly.*, **27**, 2015, 546–554.
22. VASANTHI, B.J., RAVIKUMAR, L., Synthesis and Characterization of Poly(azomethine ester)s with a Pendent DimethoxyBenzylidene Group, *Open Journal of Polymer Chemistry*, **3**, 1-8.
23. TRIPATHI, S.M., TIWARI, D., RAY, A, Electrical Conductivity of Polyazomethine Nanocomposite, *Indian Jr of Chem.*, **53A**, 2013, 1505-1512.
24. PRADEEBA S. J., SAMPATH K., A Comparative Study of Photo-Catalytic Degradation Efficiency of Methylene Blue Dye in Waste Water Using Poly(Azomethine)/ZnO Nanocomposite and Poly(Azomethine)/TiO_2 Nanocomposite, *Jr of ovo.Resea.*, 14 **(3),** 2018, 243-259.
25. PRADEEBA S. J., SAMPATH K., Photodegradation efficiency of methyl orange and Alizarin Red S in waste water using poly(azomethine)/TiO_2 nanocomposite, *AIP Conf. Proceed.*, **2162** (1), 2019, 020028.
26. PRADEEBA S. J., SAMPATH K., Synthesis and Characterization of Poly (azomethine)/ZnO Nanocomposite Toward Photocatalytic Degradation of Methylene Blue, Malachite Green, and Bismarck Brown, *Jr of Dyna. Syst., Meas.& Cont.*, **141(5**), 2019, 051001.
27. PRADEEBA S. J., SAMPATH K., Degradation of Methyl Orange and Alizarin Red S from Waste Water Using Poly(azomethine)/ZnO Nanocomposite as a Photocatalyst, *AIP Conf. Proceed.*, **2270** (1)**,** 2020, 110001.
28. PRADEEBA S. J., SAMPATH K., KALAPRIYA K., Photocatalytic Degradation Efficiency of Malachite Green in Aqueous Medium Using Poly (azomethine)/ZnO nanocomposite, *AIP Conf. Proceed.*, **2142** (1)**,** 2020, 150003.
29. PRADEEBA S. J., SAMPATH K., RAMADEVI A, Photo-catalytic Degradations of Methylene Blue, Malachite Green and Bismarck Brown Using Poly (azomethine)/TiO_2 Nanocomposite, *Clust. comp.*, **1**, 2018, 3893-3909.
30. SAMPATH KRISHNAN,, PRADEEBA, S.J., KARUNAKARAN, A., KUMARASAMY, K., MEI-CHING LIN, The effect of *p*H on the Photocatalytic Degradation of Cationic and Anionic Dyes Using Poly-azomethine/ZnO and Polyazomethine/TiO_2 Nanocomposites, *Int. Jr. of Appl. Sci.& Engg.*,**18 (5),** 2021, 1-8.
31. REDDY, K.R., PRASAD, S.B., HAN MO JEONG, ANJANAPURA V. RAGHU, Photocatalytic Activity of Titanium Dioxide-Conjugated Polymer Composite Nanoparticles Synthesized by Chemical Oxidative Polymerization, *Int. Jr of Res., Granthaalayah*, **5**, 2015, 1-6.
32. RIAZ, U., ASHRAF, S.M., KASHYAP, J, Role of Conducting Polymers in Enhancing TiO_2- based Photocatalytic Dye Degradation: A Short Review, *Poly. Plas. Tech. & Engg.*, **54**, 2015, 1850–1870.

33.SIVAKUMAR, P., PALANISAMY, P. N., Adsorption Studies of Basic Red 29 By A Nonconventional Activated Carbon Prepared from Euphorbia Antiquorum L, *Int. Jr of Chem.Tech Res.*, **1**, 2018, 502-510.
34.U. MIN, J. CHANG, Thermotropic Liquid Crystalline Polyazomethine Nanocomposites *via in situ* Interlayer Polymerization, *Mat. Chemis. & Phys.*, **129**,2011, 517–522.
35.WAHYUNI, S., KUNARTI, E. S., SWASONO, R.T., KARTINI, I, Characterization and Photocatalytic Activity of TiO_2(rod)-SiO_2-Polyaniline Nanocomposite, *Indon. Jr of Chem.*,**18 (2)**, 2018, 321 – 330.
36.WU, D., WANG, F., TAN, Y., CAOLONG, L., Facile Synthesis of NiS/CdS Nanocomposites for Photocatalytic Degradation of Quinoline under Visible Light Irradiation, *RSC Advances*, **6**, 2016, 73522-73526.
37, YONG, L., ZHANQI, G., YUEFEI, J., XIAOBIN, H., CHENG, S., SHAOGUI, Y., LIANHONG, W., QINGENG, W., FANG, D., Photodegradation of Malachite Green under Simulated and Natural Irradiation: Kinetics, Products, and Pathways, *Jr of Hazard. Mat.*, **285**, 2015, 127–136.
38.ZHU, J., JIANG, G., QIAN, F., LING, C., MING, Z, Effect of Key Operational Factors on Decolorization of Methyl Orange During H_2O_2 Assisted CdS/TiO_2/Polymer Nanocomposite thin Films under Simulated Solar Light Irradiation, *Sep. & purify. tech.*, **74**, 2010, 187-194.
39.S. M. YAKOUT, E. ELSHERIF, Batch Kinetics, Isotherm and Thermodynamic Studies of Adsorption of Strontium from Aqueous Solutions onto Low Cost Rice-straw Based Carbons, *Carbon - Sci. Tech*, **1**, 2010,144 – 153.
40. JING HE, SONG HONG, LIANG ZHANG, FUXING GAN, YUH-SHAN HO, Equilibrium and Thermodynamic Parameters of Adsorption of Methylene Blue onto Rectorite, *Fresenius Environmental Bulletin*, **19** (11 a), 2010, 2651-2656.

Mnuscript received: 26.05.2022